Semi-Three-Dimensional Analytical Torque Calculation and Experimental Testing of an Eddy Current Brake With Permanent Magnets

Kyung-Hun Shin, Hyung-Il Park, Han-Wook Cho, and Jang-Young Choi

***Abstract*—This paper presents torque analysis and testing of an eddy current brake with permanent magnets using semi-three-dimensional (3-D) analytical magnetic field calculations. The magnetic field solutions are obtained by considering the eddy current reaction using a 2-D magnetic vector potential and 3-D case by a simple and effective axial dependence modeling. The magnetic torque is also determined from these solutions. A finite-element method (FEM) is employed to validate the analytical magnetic calculations. The braking torque measurement is experimentally verified to validate the analytical study. From the experimental study, we obtain analytical and 3-D FEM results of braking torque with thermal behavior, and these are in good agreement with the experimental results.**

***Index Terms*—Analytical method, eddy current brake, permanent magnet, Maxwell stress tensor, thermal effect.**

I. Introduction

THE eddy current brake (ECB) was developed to solve problems of conventional mechanical friction brakes. Eddy currents, which are induced in nonmagnetic conductive materials due to the motion of magnetic fields, generate magnetic fields with polarity opposite to that of the applied primary fields and provide contactless retarding braking force [1], [2]. Therefore, an ECB has many advantages such as enabling a reduction in the maintenance of friction components owing to its contactless structure. In ECB with permanent magnets (PMs), the electromagnets can also be replaced by a PM, but a device such as an external system must be added to move the exciting magnetic field toward or away from the rotating parts when the braking is ON or OFF [3]. However, the electromagnetic-type ECBs that require power sources and electric control systems experience problems such as power losses [4].

Manuscript received August 29, 2017; accepted January 5, 2018. Date of publication January 18, 2018; date of current version February 2, 2018. This work was supported by the project "Development of wave energy converters applicable to breakwater and connected to microgrid with energy storage system" under Grant 20160254. *(Corresponding author: Jang-Young Choi.)*

K.-H. Shin and J.-Y. Choi are with the Department of Electrical Engineering, Chungnam National University, Daejeon 34134, South Korea (e-mail: sinkyunghun@cnu.ac.kr; choi_jy@cnu.ac.kr).

H.-I. Park is with the Advanced Brake Engineering Team, Hyundai Mobis, Giheung-gu 16891, South Korea (e-mail: hipark@mobis.co.kr).

H.-W. Cho is with the Department of Electrical, Electronics, and Communication Engineering Education, Chungnam National University, Daejeon 34134, South Korea (e-mail: hwcho@cnu.ac.kr).

Color versions of one or more of the figures in this paper are available online at http://ieeexplore.ieee.org.

Digital Object Identifier 10.1109/TASC.2018.2795010

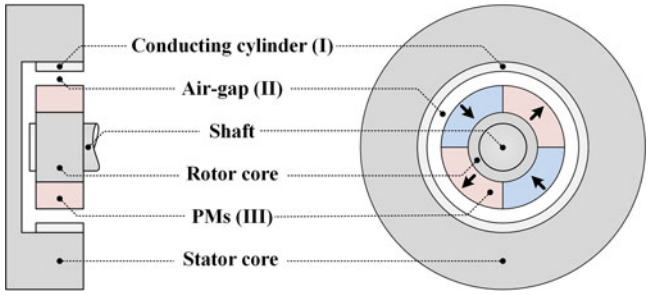

Fig. 1. Side and front views of ECB with parallel-magnetized permanent magnets.

With PM's, the machine is, therefore, mechanically more complex, but independent of any electric power source and control. This may be advantageous in some applications [3]–[5]. However, to use PMs, accurate calculations of the magnetic field are essential to predict the braking torque because it is difficult to control the magnetic field from the PMs. Accordingly, magnetic field computation using numerical analysis, such as the finite element method (FEM), is preferred [6]. However, it is generally difficult to provide straightforward physical relationships between the performance and parameters, although parametric scanning is now available by many commercial FEM packages. Thus, the analytical models are useful for understanding the fundamental physics, initial design, and optimization of the machines, while the numerical methods are good for the validation and adjustment of the design. Edwards *et al.* derived analytical braking force solutions for a linear ECB with PMs using Maxwell's equations and Fourier analysis [7]. Virtic *et al.* presented analytical torque analysis of an axial flux PM synchronous machine based on Maxwell's equations and the Maxwell stress tensor method [8]. Furthermore, Shin *et al.* derived analytical solutions of an axial PM ECB [9]. These studies prove that if the analytical magnetic field calculations are valid, they can be substituted for the FEM.

This paper presents torque characteristics analysis and experimental results for ECB with the PMs shown in Fig. 1 for analytical magnetic field calculations. The paper presents a two-dimensional(2D) solution of Maxwell equations and its extension to the three-dimensional (3D) case by a simple and effective axial dependence modeling of the magnetic field. We used the temperature measured through the experimental testing to calculate the conductivities of the conductor to obtain a good

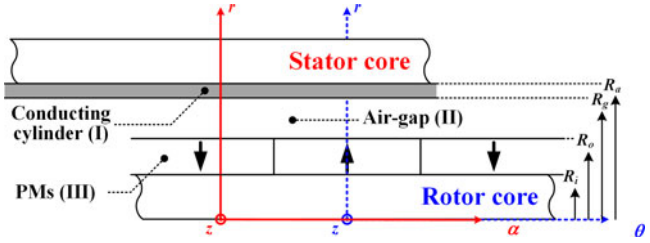

Fig. 2. Simplified multilayer analytical model.

agreement of the results. Finally, we obtained modified analytical and (3D) FEM results of braking torque with thermal behavior, which were found to be in good agreement with the experimental results.

II. Analytical Magnetic Field Calculations

A. Analytical Model

Fig. 2 shows the simplified multilayer analytical model used for the magnetic field calculations. The rotor is rotated based on the (*r, θ, z*) coordinate system, and the stator is fixed based on the (*r, α, z*) coordinate system. Here, θ and α are angular components, and their relationship is given by $\theta = \alpha + \omega_r t$, where ω_r (rad/s) is the angular speed of the rotor. To derive the magnetic field, we consider the analytical model to be composed of three regions: the conducting cylinder (I), the air gap (II), and the PMs (III). In region (I), R_a and R_g denote the outer and inner radii of the conducting cylinder, respectively. The permeability of the conducting cylinder is assumed to be equal to that of free space, μ_0, and the conductivity of the conducting cylinder is denoted by σ_{al}. In region (III), R_o and R_i denote the outer and inner radii of the PMs, respectively. The permeability of the PMs is also assumed to be equal to μ_0, and the conductivity of the PMs is assumed to be zero because eddy current is not induced in the magnets. Moreover, the relative permeability of the stator and rotor cores are infinite, and their conductivities are assumed to be zero because of their laminated structure.

B. Magnetic Field Distributions

The governing equations are obtained from $\mathbf{B} = \mu_0(\mathbf{H} + \mathbf{M})$, where ($\mathbf{B}$) and ($\mathbf{H}$) are the magnetic flux density and the magnetic intensity, respectively. In region (I), $\mathbf{M} = 0$ and $\mathbf{B} = \mu_0\mathbf{H}$ because of the absence of magnetization. By applying the curl operator to both sides of this equation, we obtain $\nabla \times \mathbf{B} = \mu_0(\nabla \times \mathbf{H})$. This equation can be rewritten as $\nabla \times (\nabla \times \mathbf{A}) = \mu_0\mathbf{J}$ using the definition of the magnetic vector potential $\nabla \times \mathbf{A} = \mathbf{B}$, and the current density generated by the rotor PMs $\mathbf{J} = \nabla \times \mathbf{H}$.

The current density can be expressed as $\mathbf{J} = \sigma_{al}\mathbf{E}$, and the electric field intensity ($\mathbf{E}$) is expressed using Faraday's law as

$$\nabla \times \mathbf{E} = -\frac{\partial \mathbf{B}}{\partial t} = -\frac{\partial(\nabla \times \mathbf{A})}{\partial t} = \nabla \times \left(-\frac{\partial \mathbf{A}}{\partial t}\right) \tag{1}$$

Equation (2) can be written using (1) as Poisson's equation:

$$\nabla^2 \mathbf{A^I} = \mu_0 \sigma_{al} \frac{\partial \mathbf{A^I}}{\partial t} \tag{2}$$

The superscript I denotes the conducting cylinder region.

In region (II), $\nabla \times \mathbf{B} = 0$ because $\nabla \times \mathbf{H} = 0$ and $\mathbf{M} = 0$ owing to the absence of the free current and the magnetization. In region (III), $\nabla \times \mathbf{H} = 0$ and $\nabla \times \mathbf{B} = \mu_0(\nabla \times \mathbf{M})$ owing to the absence of free currents. Similarly, the equations for the other regions are obtained as follows:

$$\begin{aligned} \nabla^2 \mathbf{A^{II}} &= 0 \\ \nabla^2 \mathbf{A^{III}} &= -\mu_0(\nabla \times \mathbf{M}) \end{aligned} \tag{3}$$

The superscripts II and III denote the air-gap and magnet regions, respectively. The mathematical expression for the magnetization of the parallel-magnetized PMs is represented using Fourier series as

$$\mathbf{M} = \sum_{n=-\infty,odd}^{\infty} (M_{rn}\mathbf{i_r} + M_{\theta n}\mathbf{i}_\theta) e^{-jnp\theta} \tag{4}$$

where M_{rn}, $M_{\theta n}, n$, and p denote the amplitudes of the *n*th order normal and tangential magnetization components, *n*th order space harmonic, and pole pairs, respectively. The Fourier coefficients and analytical model for parallel magnetization are presented in [10].

The vector potential ($\mathbf{A}$) can be expressed as $\mathbf{A} = \Sigma A_n(r) e^{-jnp(\alpha or\, \theta)}\mathbf{i_z}$. Therefore, (2) and (3) can be rewritten as

$$\begin{aligned} \mathbf{A^I} &= \sum_{n=-\infty,odd}^{\infty} \left\{C_n^I I_{np}(\beta_n r) + D_n^I K_{np}(\beta_n r)\right\} e^{-jnp\alpha}\mathbf{i_z} \\ \mathbf{A^{II}} &= \sum_{n=-\infty,odd}^{\infty} \left\{C_n^{II} r^{np} + D_n^{II} r^{-np}\right\} e^{-jnp\theta}\mathbf{i_z} \\ \mathbf{A^{III}} &= \sum_{n=-\infty,odd}^{\infty} \left\{C_n^{III} r^{np} + D_n^{III} r^{-np} - \frac{\mu_0 M_n}{1-(np)^2} r\right\} e^{-jnp\theta}\mathbf{i_z} \end{aligned} \tag{5}$$

where $\beta_n^2 = jnp\mu_0\sigma_{al}\omega_r$, $M_n = jnpM_{rn} + M_{\theta n}$, and I_{np} and K_{np} are the modified Bessel functions of the first and second kind of order *np*, respectively.

The undefined coefficients $C_n^I, C_n^{II}, C_n^{III}, D_n^I, D_n^{II}$, and D_n^{III} in (5) can be determined using the boundary conditions provided in [11].

C. Semi-3D Analytical Method

In the case of small air-gap machines, the edge effects are usually neglected, and the radial dependence of the magnetic field is not considered. However, in the case of ECB with PMs, the mechanical constraints due to ON or OFF and to the radial forces between stator and rotor require a relatively large mechanical air gap. Consequently, one cannot neglect the radial dependence of the air-gap magnetic field [12].

In order to consider the end effects to the z-direction, this paper introduces a correction function in (6) that gives precise values for the magnetic field.

$$G(z) = \sum_{m=1}^{5} a_m e^{-\left(\frac{z-b_m}{c_m}\right)^2} \tag{6}$$

where $\mathrm{a_m}$, $\mathrm{b_m}$, and $\mathrm{c_m}$ are the *m*th unknown parameters.

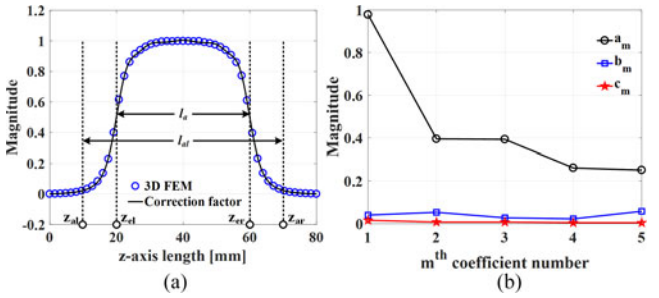

Fig. 3. (a) Results of correction function for semi-3D analytical method and (b) coefficients for semi-3D analytical method.

Thus, the correction function can be obtained using the FEM according to the z-direction, as shown in Fig. 3.

The flux density (**B**) is obtained from the definition of magnetic vector potential, $\nabla \times \mathbf{A} = \mathbf{B}$. The normal ($\mathbf{B_r}$) and tangential ($\mathbf{B}_\theta$) flux density in each region are expressed as

$$\mathbf{B}_{\mathbf{r}}^{\mathbf{I,II,III}} = -G(z) \times \sum_{n=-\infty,odd}^{\infty} \frac{jnp}{r} A_n^{I,II,III}(r) e^{-jnp(\alpha or\theta)} \mathbf{i_r}$$

$$\mathbf{B}_{\theta}^{\mathbf{I,II,III}} = -G(z) \times \sum_{n=-\infty,odd}^{\infty} \frac{\partial A_n^{I,II,III}(r)}{\partial r} e^{-jnp(\alpha or\theta)} \mathbf{i}_\theta \tag{7}$$

D. Braking Torque Analysis

The magnetic force (**F**) produced by the interaction between the conducting cylinder and the PMs is derived using the Maxwell stress tensor [13].

$$\mathbf{F} = -S\left\langle T_{r\theta}^{r=R_g} \right\rangle_\theta = -S\mu_0 \left\langle \mathbf{H_r^I}(R_g,\theta)\, \mathbf{H}_\theta^{\mathbf{I}}(R_g,\theta) \right\rangle_\theta$$

$$= -\frac{1}{\mu_0} \int_{z_{al}}^{z_{ar}} \int_0^{2\pi} G(z)^2 \mathbf{B_r^I}(R_g,\theta) \cdot \left(\mathbf{B}_\theta^{\mathbf{I}}(R_g,\theta)\right)^* R_g \, d\theta dz \tag{8}$$

where the angled brackets $<\cdot>_\theta$ denote the spatial average at θ of the quantity enclosed by the brackets.

The inner surface area of the conducting plate ($r = R_g$), which encloses an integer number of periods, is $S = 2\pi R_g l_{al}$, where l_{al} is the active length of the conducting cylinder. The superscript $*$ denotes the complex conjugate. As a result, the torque (**T**) can be calculated using the relation $\mathbf{T} = R_g \mathbf{F}$.

III. Results and Discussions

A. Comparison of Predictions With FEM Results

Fig. 4 shows the flux line distributions of the ECB with parallel magnetized PMs obtained from FEM calculations at 0 rpm and 3000 rpm. The magnetic flux lines are distorted depending on the rotation of the PMs because of the eddy current reaction. This phenomenon can also be seen in Fig. 5, which shows the comparison of the analytical results with the FEM results for the flux density at $r = R_g$. As shown, the magnetic flux density curve is distorted at 3000 rpm because of the eddy current reaction. In Fig. 6, the presented results are the normal and tangential flux density along the z-axis, and they were obtained by the semi-3D analytical method.

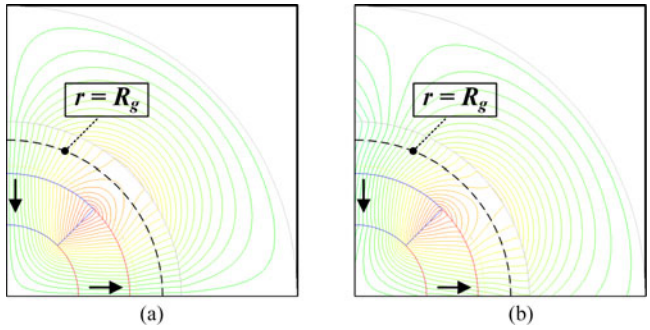

Fig. 4. Flux line distributions obtained using FEM at (a) 0 rpm and (b) 3000 rpm.

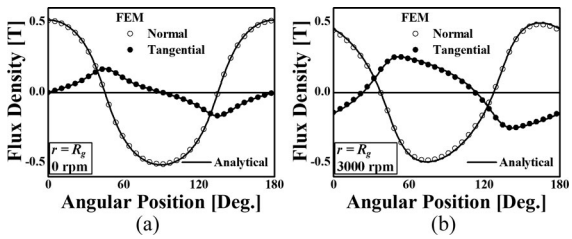

Fig. 5. Comparison of analytical and FEM results of flux density of the initial model presented in Fig. 4 at (a) 0 rpm and (b) 3000 rpm.

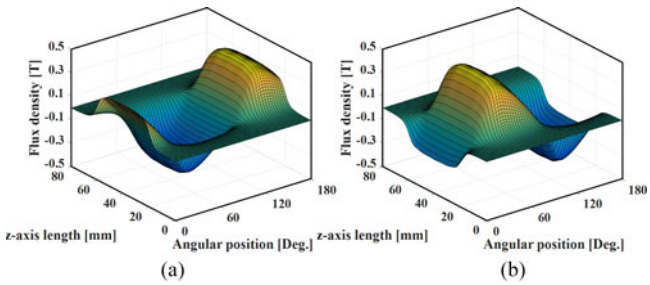

Fig. 6. Semi-3D analytical results of flux density distribution at 3000 rpm: (a) normal and (b) tangential component.

B. Comparison of Predictions With FEM Results

Fig. 7 shows the testing apparatus for measuring the magnetic torque of the ECB with parallel magnetized PMs. It comprises an ECB, speed sensor, torque sensor, and driving motor with a rotational speed of up to 3000 rpm and an acceleration of 100 rpm/s^2. We used sintered neodymium iron boron (NdFeB) magnets in the rotor, and it was assembled in the nonmagnetic metal frame to prevent scattering of the PMs.

The specifications of the components are listed in Table I.

In the actual test, the induced eddy currents increase as the rotor speed increases. Moreover, they generate heat and increase the resistivity of the conducting cylinder. Therefore, an efficient cooling system must be used. The torque measurement results and the analytical and FEM results are shown in Fig. 8. We can see that the measured values decrease compared with the predicted values because the testing setup was equipped with only a forced air-cooling system, which is incapable of

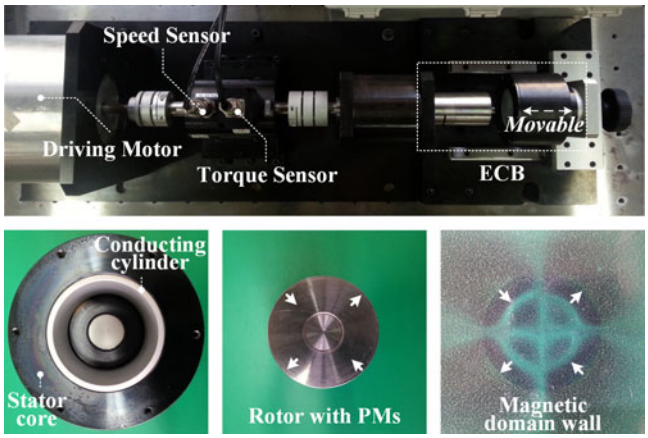

Fig. 7. Testing apparatus to measure the braking torque.

TABLE I
SPECIFICATIONS OF THE TESTING APPARATUS

Symbol	Designation	Value	Unit
t_m	Thickness of the PMs	8	mm
R_o	Outer radius of the PMs	19	mm
R_i	Inner radius of the PMs	11	mm
B_r	Residual magnetic flux density	1.3	T
t_c	Thickness of the conducting cylinder	3	mm
R_a	Outer radius of the conducting cylinder	27	mm
R_g	Inner radius of the conducting cylinder	24	mm
σ_{al}	Conductivity of the conducting cylinder	1.4e7	S/m
l_a	Active length of the rotor	40	mm
l_{al}	Active length of conducting cylinder	60	mm
P	Number of pole-pairs	2	

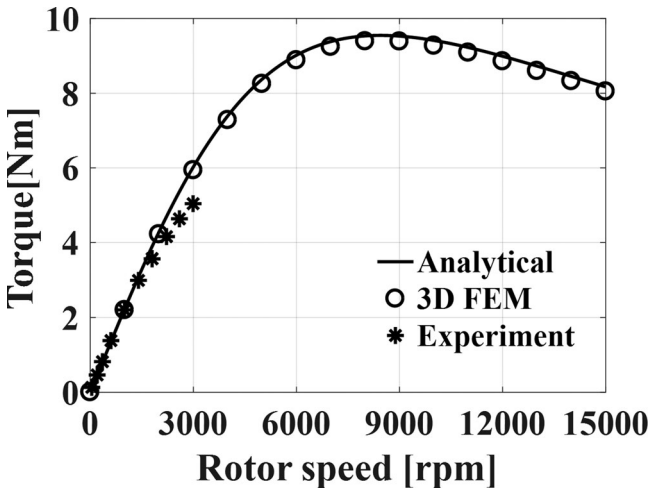

Fig. 8. Analytical, FEM, and experimental results of braking torque of the actual PM type ECB model.

efficiently removing the heat generated by the induced eddy currents, and the analytical and FEM analyses do not consider the thermal behavior. Actually, it is very complicated to predict temperature rise due to eddy current in a conducting cylinder. Therefore, we used the measured temperature obtained from the experimental testing to calculate the conductivities of the conductor for exact agreement of the results, as shown in Fig. 9.

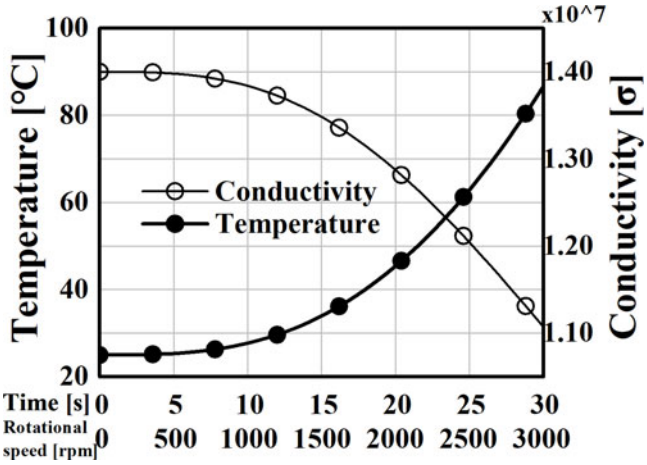

Fig. 9. Variation of measured temperature rise with conductivity in conducting cylinder.

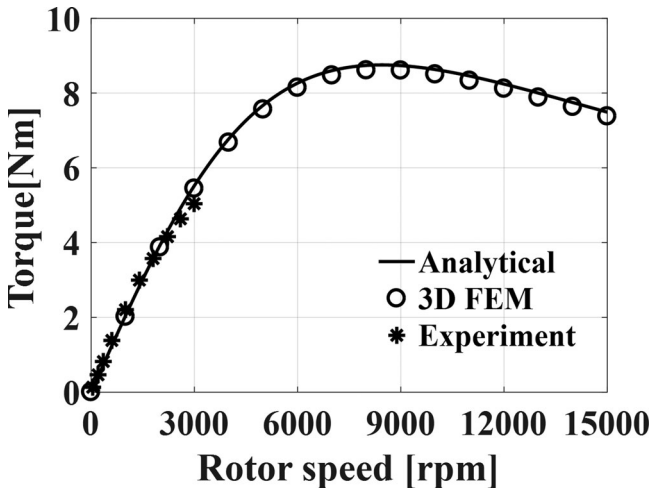

Fig. 10. Modified analytical, FEM, and experimental results of braking torque of the actual PM type ECB model with thermal behavior.

Finally, we obtained modified analytical and FEM results of braking torque with thermal behavior, and these are in good agreement with the experimental results, as shown in Fig. 10.

IV. CONCLUSION

In this study, the torque calculation of an ECB with PMs was analyzed using magnetic field calculations. The magnetic field solutions were obtained using a 2D magnetic vector potential and its extension to the 3D case by a simple and effective axial dependence modeling of the magnetic field. The magnetic torque was also derived from these solutions. 3D FEM and experimental testing were employed to validate the results of the analysis. The induced eddy currents heated and increased the resistivity of the conducting cylinder.

Therefore, we used the temperature measured from the experimental testing to calculate the conductivities of the conductor to achieve an exact agreement of the results. From experimental study, we obtained modified analytical and FEM results of braking torque with thermal behavior, and these were in good agreement with the experimental results. The analytical

method proposed here should be very useful in initial design and optimization process of an ECB with PMs.

REFERENCES

[1] S. E. Gay and M. Ehsani, "Analysis and experimental testing of a permanent magnet eddy-current brake," in *Proc. IEEE Veh. Power Propulsion Conf.*, 2005, pp. 756–765.

[2] Z. Mouton and M. J. Kamper, "Modeling and optimal design of an eddy current coupling for slip-synchronous permanent magnet wind generators," *IEEE Trans. Ind. Electron.*, vol. 61, no. 7, pp. 3367–3376, Jul. 2014.

[3] B. Lequesne, B. Liu, and T. W. Nehl, "Eddy-current machines with permanent magnets and solid rotors," *IEEE Trans. Ind. Appl.*, vol. 33, no. 5, pp. 1289–1294, Sep./Oct. 1997.

[4] S.-M. Jang, S.-H. Lee, and S.-S. Jeong, "Characteristic analysis of eddy-current brake system using the linear Halbach array," *IEEE Trans. Magn.*, vol. 38, no. 5, pp. 2994–2996, Sep. 2002.

[5] J. E. Gould, "Permanent magnet applications," *IEEE Trans. Magn.*, vol. MAG-5, no. 4, pp. 812–821, Dec. 1969.

[6] J. Y. Choi, H. J. Shin, S. M. Jang, and S. H. Lee, "Torque analysis and measurements of cylindrical air-gap synchronous permanent magnet couplings based on analytical magnetic field calculations," *IEEE Trans. Magn.*, vol. 49, no. 7, pp. 3921–3924, Jul. 2013.

[7] J. D. Edwards, B. V. Jayawant, W. R. C. Dawson, and D. T. Wright, "Permanent-magnet linear eddy-current brake with a nonmagnetic reaction plate," *Proc. IEE*, vol. 146, no. 6, pp. 627–631, Nov. 1999.

[8] P. Virtic, P. Pišek, M. Hadžiselimović, T. Marcic, and B. Stumberger, "Torque analysis of an axial flux permanent magnet synchronous machine by using analytical magnetic field calculation," *IEEE Trans. Magn.*, vol. 45, no. 3, pp. 1036–1039, Mar. 2009.

[9] H.-J. Shin, J.-Y. Choi, H.-W. Cho, and S.-M. Jang, "Analytical torque calculations and experimental testing of permanent magnet axial eddy current brake," *IEEE Trans. Magn.*, vol. 49, no. 7, pp. 4152–4155, Jul. 2013.

[10] Z. Q. Zhu, D. Howe, and C. C. Chan, "Improved analytical model for predicting the magnetic field distribution in brushless permanent-magnet machines," *IEEE Trans. Magn.*, vol. 38, no. 1, pp. 229–238, Jan. 2002.

[11] J.-Y. Choi, H.-Y. Kim, S.-M. Jang, and S.-H. Lee, "Thrust calculations and measurements of cylindrical linear actuator using transfer relations theorem," *IEEE Trans. Magn.*, vol. 44, no. 11, pp. 4081–4084, Nov. 2008.

[12] H. Tiegna, Y. Amara, and G. Barakat, "A new quasi-3–D analytical model of axial flux permanent magnet machines," *IEEE Trans. Magn.*, vol. 50, no. 2, Feb. 2014, Art. no. 7020204.

[13] J. R. Melcher, *Continuum Electromechanics*. Cambridge, MA, USA: MIT Press, 1981.